Synchrotron X-ray Scattering Characterization of the Molecular Structures of Star Polystyrenes with Varying Numbers of Arms

Sangwoo Jin,[†,‡] Tomoya Higashihara,[†,§] Kyeong Sik Jin,[∥] Jinhwan Yoon,[‡] Yecheol Rho,[‡] Byungcheol Ahn,[‡] Jehan Kim,[∥] Akira Hirao,[*,§] and Moonhor Ree[*,⊥,‡]

Department of Chemistry, National Research Lab for Polymer Synthesis & Physics, Center for Electro-Photo Behaviors in Advanced Molecular Systems, BK School of Molecular Science, Division of Advanced Materials Science, and Polymer Research Institute, Pohang University of Science & Technology (POSTECH), Pohang 790-784, Republic of Korea, Polymeric and Organic Materials Department, Graduate School of Science and Engineering, Tokyo Institute of Technology, H-127, 2-12-1, Ohokayama, Meguro-ku, Tokyo 152-8552, Japan, and Pohang Accelerator Laboratory, Pohang University of Science & Technology (POSTECH), Pohang 790-784, Republic of Korea

Received: December 17, 2009; Revised Manuscript Received: April 12, 2010

We have synthesized well-defined multiarmed star polystyrenes, with 6, 9, 17, 33, and 57 arms, and studied their molecular shapes and structural characteristics in a good solvent (tetrahydrofuran at 25 °C) and in a theta (Θ) solvent (cyclohexane at 35 °C) by small-angle X-ray scattering (SAXS) using a synchrotron radiation source. Analysis of the SAXS data provided a detailed characterization of the molecular shapes, including the contributions of the blob morphology of the arms, the radius of gyration, the paired distance distribution, the radial electron density distribution, and the Zimm−Stockmayer and Roovers *g*-factor, for the multiarmed star polystyrenes. In particular, the molecular shapes of the star polystyrenes were found to change from a fuzzy ellipsoid, for the 6-armed polystyrene, to a fuzzy sphere, for the 57-armed polystyrene, with an increasing number of arms. The ellipsoidal character of the star polystyrenes with fewer arms may originate from the extended anisotropically branched architecture at the center of the molecule. The arms of the star polystyrenes were found to be more extended than those of the linear polystyrenes. Furthermore, the degree of chain extension in the arms increased with the number of arms.

Introduction

Star polymers can be capped with a variety of end groups to yield high functionality and are therefore of interest in both academia and industry.[1–5] These multifunctional advantages have inspired development of several synthetic strategies for achieving star polymers.[6–12] Their structural properties have been characterized in solutions composed of both good and theta (Θ) solvents[11–19] and have been examined using a variety of techniques, such as light scattering,[20,21] small angle neutron scattering,[21–23] and viscometry.[24,25] The physical properties of star polymers have also been studied theoretically using Monte Carlo methods.[26] However, the previous experimental studies have been restricted to star polymers with a limited numbers of arms, because the synthesis of star polymers with higher numbers of arms has, in the past, proven to be difficult.[6,8,14]

In this study, we investigated the structures of a series of well-defined star polystyrenes (star-PS), bearing up to 57 arms, in good and Θ solvents using synchrotron small-angle X-ray scattering (SAXS) techniques. The SAXS data were primarily analyzed using a model-free indirect Fourier transform (IFT) method, which required only an estimate of the maximum dimension of the scatterers.[27–30] The scattering data were also analyzed using a variety of structural models, including the Gaussian chain, hard sphere, fuzzy sphere, and fuzzy ellipsoid models. Tetrahydrofuran (THF) at 25 °C and cyclohexane at 35 °C were used as the good solvent and the Θ solvent, respectively. Quantitative scattering analysis strongly suggested that the star-PS polymer shapes progress continuously from a fuzzy ellipsoid to a fuzzy sphere, as the number of arms increases. Moreover, the polymeric behavior of the star-PS polymers was found to depend on the solvent conditions.

TABLE 1: Molecular Weights, Polydispersity Indices, and Sizes of the Linear-PS Polymers

			$\bar{R}_{g,G}$[b] (Å)	
linear-PS	$\bar{M}_w$ ($\times 10^3$)	DPI[a]	THF	cyclohexane
F-1	9.83	1.02	28	24
F-2	19.6	1.01	42	34
F-4	43.9	1.01	59	50

[a] Polydispersity index ($=\bar{M}_w/\bar{M}_n$): $\overline{M_w}$ and $\bar{M}_n$ are the weight- and number-averaged molecular weights, respectively. [b] Average radius of gyration was obtained from the Guinier analysis of the scattering data.

Experimental Section

Three different linear-PS materials were used in this study, which were purchased from Varian, Inc. Their molecular weight data are listed in Table 1. Five star-PS polymers with 6-, 9-,

* To whom correspondence should be addressed. E-mail: ree@postech.edu (M.R.), ahirao@polymer.titech.ac.jp (A.H.). Tel: +82-54-279-2120 (M.R.), +81-3-5734-2131 (A.H.).

† S.J. and T.H. contributed equally to this study.

‡ Department of Chemistry, National Research Lab for Polymer Synthesis & Physics, Center for Electro-Photo Behaviors in Advanced Molecular Systems, BK School of Molecular Science, Division of Advanced Materials Science, and Polymer Research Institute, Pohang University of Science & Technology.

§ Tokyo Institute of Technology.

∥ Pohang Accelerator Laboratory, Pohang University of Science & Technology.

10.1021/jp911928b
Published on Web 04/28/2010

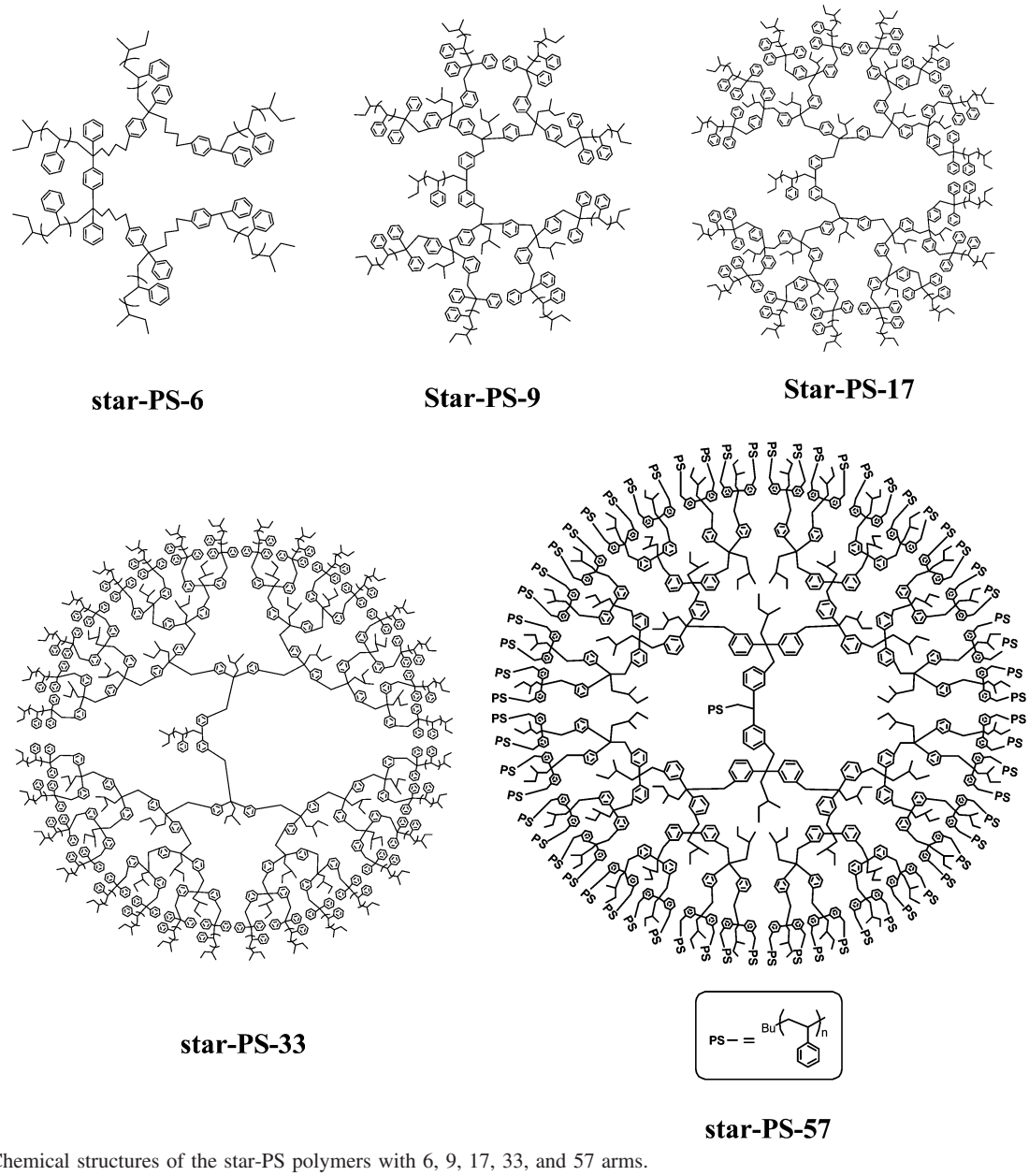

Figure 1. Chemical structures of the star-PS polymers with 6, 9, 17, 33, and 57 arms.

TABLE 2: Molecular Weights, Polydispersity Indices, and Structural Parameters of the Star-PS Polymers

				THF				cyclohexane				
star-PS	arm number	$\bar{M}_w$ ($\times 10^4$)	DPI[a]	$R_{g,IFT}$[b] (Å)	$\bar{R}_{g,G}$[c] (Å)	$\bar{R}_g$ (Å)	g[f]	$R_{g,IFT}$[b] (Å)	$\bar{R}_{g,G}$[c] (Å)	$\bar{R}_g$ (Å)	g[f]	g[h]
star-PS-6	6	6.88	1.03	38.0	46.6	48.9[d]	0.44	34.2	40.8	41.2[d]	0.43	0.44
star-PS-9	9	10.2	1.04	46.0	52.4	49.5[d]	0.31	38.3	44.1	41.9[d]	0.34	0.31
star-PS-17	17	11.2	1.02	34.7	38.7	38.3[d]	0.17	30.2	33.1	32.5[d]	0.18	0.17
star-PS-33	33	18.6	1.03	41.8	45.0	44.3[e]	0.14	36.9	39.6	37.8[e]	0.15	0.14
star-PS-57	57	31.3	1.03	47.1	47.6	45.5[e]	0.09	41.8	42.9	39.0[e]	0.11	0.09

[a] Polydispersity index ($=\bar{M}_w/\bar{M}_n$): $\bar{M}_w$ and $\bar{M}_n$ are the weight- and number-averaged molecular weights, respectively. [b] Radius of gyration was obtained from the IFT method. [c] Average radius of gyration was calculated from the Guinier fit. [d] Theoretical radius of gyration was estimated from g-factor by the Zimm−Stockmayer theory. [e] Theoretical radius of gyration was estimated from g-factor by the Roovers theory. [f] g-factor was calculated from eq 8 and the radius of gyration of the linear-PS with a same molecular weight. [h] g-factor estimated from either the Zimm−Stockmayer theory or the Roovers theory.

17-, 33-, and 57-arms were synthesized by coupling reaction of polymer anions consisting of two polymer chains with chain-end-multifunctionalized polystyrenes with benzyl bromide moieties as reported previously in the literature.[3,31] Their chemical structures are shown in Figure 1. The weight- and number-average molecular weights ($\bar{M}_w$ and $\bar{M}_n$) of all the star-PS materials were measured by using vapor pressure osmometry and static light scattering. The $\bar{M}_w$ and $\bar{M}_n$ results are summarized in Table 2. For these star- and linear-PS polymers, a series of solution samples were prepared at a concentration of mass fraction ≤4% in THF at 25 °C (good solvent) and in cyclohexane at 35 °C (Θ solvent). SAXS measurements were conducted at the 4C1 beamline of the Pohang Light Source (PLS) facility with 2.5 GeV power in the Pohang University of

Science and Technology.[29,30,32,33] X-ray beams from a bending magnet of the PLS storage ring were focused by toroidal silicon mirrors coated with platinum and monochromatized with using a W/B_4C double multilayer monochromator. The wavelength and size of the monochromatized X-ray beam were 1.608 Å and 0.6×0.6 mm^2 respectively, and an evacuated scattering path with Kapton windows and the sample-to-detector distances (SDD) of 1.0, 2.0, and 3.0 m were used. SAXS data were measured using a two-dimensional (2D) charge-coupled device (CCD) detector (model MAR165, Mar USA, Evanston, IL). Solution sample cells with 10 μm thick mica windows and an X-ray beam path length of 0.7 mm were used. A sample cell chamber equipped with an Eurotherm controller and a K-type thermocouple was used to control the temperature of solution sample cells. The scattering angle was calibrated with linear polyethylene, collagen (chicken tendon), polystyrene-*b*-polyethylene-*b*-polybutadiene-*b*-polystyrene, and silver behenate standards. Each 2D SAXS pattern was circular averaged from the beam center, then normalized to the transmitted X-ray beam intensity, which was monitored with a scintillation counter placed behind the sample, and corrected for the scattering due to the used solvent.

Results and Discussion

The scattering intensity $I(q)$ from globular particles in a solvent medium can be expressed by the following equation:[27–30,32,33]

$$I(q) = kNP(q)\,S(q) \quad (1)$$

where k is a constant, N is the number of particles, $P(q)$ is the form factor of a single particle, and $S(q)$ is the structure factor. Here q is the magnitude of the scattering vector defined as $q = 4\pi \sin\theta/\lambda$, where 2θ is the scattering angle. The term $P(q)$ provides information on the particle shape and size, while the term $S(q)$ describes the interparticle distances in solution. In general, for dilute solutions, the term $S(q)$ can be approximated as unity over the entire q range, and indeed, the term $P(q)$ can be directly obtained from the scattering intensity $I(q)$, yielding the particle shape and size. The scattering intensity from a dilute solution is usually detectable in the low q region but is very weak in the high q region. Thus, the intensity is easily obscured by the background noise, producing significant errors in analysis of the scattering data. To overcome this problem, semidilute solutions are often used assuming that the approximation $S(q) \approx 1$ holds over the entire q range.

In this study we conducted SAXS measurements on the solutions of both linear- and star-PS polymers in THF at 25 °C (good solvent) and in cyclohexane at 35 °C (Θ solvent) over the concentration range ≤4.0 wt % to find an appropriate polymer concentration to give good quality scattering data without contribution of the structure factor $S(q)$ in eq 1. The SAXS data analysis found that the contribution of the term $S(q)$ was negligible for the SAXS data obtained with a polymer concentration of 1.0−4.0 wt %. Even for only 1.0 wt % polymer solutions, good quality SAXS data were obtainable. Therefore, in this study all SAXS measurements were carried out with 1.0 wt % (dilute) polymer solutions. Furthermore, in our study the IFT method[27–30] was adopted and used to analyze the measured scattering data for several reasons. First, the IFT method does not assume a scattering model during data analysis. Second, IFT smoothes the primary data by a weighted least-squares procedure, estimates the optimal stabilization parameter based on a stability plot, and transforms the data into real space. Finally, the method minimizes the impact of missing data and, therefore, accurately provides the pair distance distribution function $p(r)$ or, equivalently, the correlation function $\gamma(r) = r^{1-dim}\rho(r)$, where r is the distance between the paired scattering elements in the polymer molecule, *dim* defines the type of symmetry (*dim* = 1, lamellar; *dim* = 2, cylindrical; and *dim* = 3, spherical) and $\rho(r)$ is the radial electron density distribution function. The scattering data were also analyzed using several models (Gaussian chain, hard sphere, fuzzy sphere, fuzzy ellipsoid) and other methods, to obtain a detailed description of the structural properties of the star-PS polymers in solution. These properties were compared with those of linear-PS polymers.

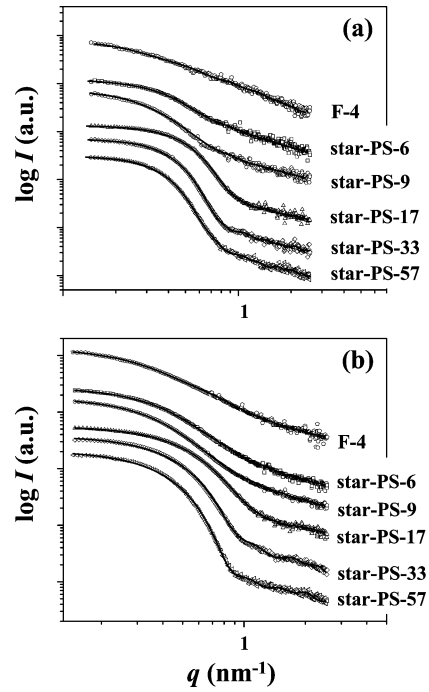

Figure 2. SAXS profiles of the linear-PS (F-4) and star-PS polymers (star-PS-6 through star-PS-57) obtained under (a) THF (good solvent) and (b) cyclohexane (Θ solvent). The symbols indicate the measured data, and the solid lines indicate the IFT fits. The concentrations of the polymer solutions were 1.0 wt %.

Linear-PS. Representative solution SAXS profiles of linear-PS polymers are presented in Figure 2. These profiles were collected from linear-PS (F-4) in both good and Θ solvents. Similar scattering profiles were observed for other linear-PS polymers with varying molecular weights (data not shown). As can be seen in Figure 2, the model-independent IFT method fit both scattering profiles well. The scattering profile in THF followed a power law $q^{-5/3}$ in the intermediate q region (Debye region) as well as in the high q region (Porod region). On the other hand, the scattering profile in cyclohexane followed a power law q^{-2} in both the intermediate and high q regions. These scattering characteristics suggested that linear-PS in the good solvent behaved as a wormlike chain with the arms diffusing as a self-avoiding random walk, whereas linear-PS in the Θ solvent behaved as a Gaussian chain subject to excluded volume effects.[12,27] These results were in good agreement with those reported in the literature.[34] The size distribution of the linear-PS polymers was determined from the scattering profiles in the low q region by Guinier analysis.[27] The results are listed in Table 1.

6-Armed Star-PS (Star-PS-6). The SAXS profiles of the star-PS-6 in THF as well as in cyclohexane are shown in Figure 2. The scattering profiles in the low q region yielded an average radius of gyration ($\bar{R}_{g,G}$) from fits to the Guinier equation,[27]

$$\ln I(q) = \ln I_o - R_g^2 q^2/3 \quad (2)$$

for $qR_g \ll 1$. That is, a Guinier fit of $\ln[I(q)]$ vs q^2 yielded an estimate for $\bar{R}_{g,G}$ from the initial slope of the curve at $q \approx 0$. The radius of gyration ($R_{g,IFT}$) can also be obtained from the measured intensity $I(q)$ using IFT analysis with the following relation:[27–30]

$$I(q) = 4\pi \int_0^\infty p(r) \frac{\sin(qr)}{qr} \, dr \quad (3)$$

where $p(r)$ is the pair distance distribution function, which gives the probability of finding two scattering elements separated by a distance r in the interior of a polymer molecule. The $p(r)$ in eq 3 yields an estimate for $R_{g,IFT}$ by the following relation:

$$R_g^2 = \frac{\int_0^\infty p(r) r^2 \, dr}{2 \int_0^\infty p(r) \, dr} \quad (4)$$

Using the above Guinier and IFT methods, the size distributions (i.e., $\bar{R}_{g,G}$ and $R_{g,IFT}$) of star-PS-6 in THF and cyclohexane were determined from the measured SAXS profiles. The results are listed in Table 2. The star-PS-6 polymer had a larger value of $\bar{R}_{g,G}$ in THF than in cyclohexane, as expected, because THF and cyclohexane are good and Θ solvents, respectively, for the PS arm segments. Furthermore, the results showed that the value of $R_{g,IFT}$ was significantly smaller than the value of $\bar{R}_{g,G}$, indicating that the star-PS-6 molecule was not a perfectly homogeneous particle that has equal size and shape; namely, the star-PS-6 polymer in solution gradually drifts apart from a homogeneous particle.

The solution properties of star-PS-6 were analyzed using the g-factor.[35] The g-factor provides a relationship between the values of R_g for the star-PS and the linear-PS. In general, star-PS is more compact in size and shape than linear-PS of the same molecular weight and chemical composition. Star-PS has a higher segment density than its linear counterpart. Therefore, the R_g for star-PS are expected to be smaller than linear-PS with the same molecular weight under the same conditions. The relationship between the g-factor and the R_g can be expressed as follows:

$$g = \langle \bar{R}_g^2 \rangle_{star} / \langle \bar{R}_g^2 \rangle_{linear} \quad (5)$$

where $\langle \bar{R}_g^2 \rangle_{star}$ and $\langle \bar{R}_g^2 \rangle_{linear}$ are the averaged square of the radii of gyration of, respectively, star- and linear-PS in the same solvent conditions. The average radii of gyration ($\langle \bar{R}_g^2 \rangle_{star}^{1/2}$) of star-PS-6 in good and Θ solvents were determined from the scattering data analysis (Table 2). The averaged radius of gyration ($\langle \bar{R}_g^2 \rangle_{linear}^{1/2}$) for linear-PS, in good and Θ solvents, was obtained from the weight-average molecular weight $\bar{M}_w$ using the following relations, respectively:[35]

$$\langle \bar{R}_g^2 \rangle_{linear}^{1/2} = 0.363 \bar{M}_w^{0.477} \quad (6)$$

$$\langle \bar{R}_g^2 \rangle_{linear}^{1/2} = 0.274 \bar{M}_w^{0.487} \quad (7)$$

These relations were also used to obtain the g-factors of star-PS-6, listed in Table 2.

The theoretical g-factors were calculated using the relations proposed by Zimm−Stockmayer (for arm numbers ≤17) (eq 8)[35–37] and Roovers (for arm number >17) (eq 9):[38]

$$g = (3f - 2)/f^2 \quad (8)$$

$$\log g = 0.36 - 0.80 \log f \quad (9)$$

where f is the number of arms. In addition, the theoretical values of R_g for star-PS-6 in both solvents were calculated using eqs 5−8. The results are listed in Table 2.

Table 2 shows that the g values and molecular sizes of the star-PS-6 polymers in either solvent agreed with the theoretical values. The agreement between theoretical and experimental parameters indicated that star-PS-6 in good and Θ solvents assumed a starlike molecular shape.

The solution properties can be obtained from the measured scattering profiles. In the intermediate q region, which is related to the molecular shape, the scattering profile of star-PS-6 in THF was found to follow a q^{-2} power law, indicating that star-PS-6 in good solvents assumed a molecular shape that resembled a soft sphere rather than a hard sphere. This result was reasonable in light of the polymer's chemical structure. Figure 1 shows that the arms were separated by a significant quantity of free space, which allowed the star-PS-6 polymers to form a soft inner structure. The star-PS-6 polymer in cyclohexane also followed a q^{-2} power law in the intermediate q region of the scattering profile. Star-PS-6 apparently retained a soft sphere shape in the Θ solvent, although the molecular size was observed to be smaller than in the good solvent, and star-PS-6 molecules in the Θ solvent assumed a shape that deviated from spherical. The scattering profile Kratky representations, shown in Figure 3, revealed that star-P-6, in both good and Θ solvents, did not present a first maximum at $qR_g \approx 1.49$, which is, in general, characteristic of isotropic spheres. The molecular shape of star-PS-6 in both solvents probably deviated from spherical, and was more likely to be ellipsoidal.

In the high q region, the scattering profiles of star-PS-6 in both solvents followed a power law $q^{-5/3}$. This behavior indicated that star-PS-6 in both good and Θ solvents had no sharp interfaces with the solvent media. Star-PS-6 most likely displayed "fuzziness", defined as the ratio of the shell thickness to the core radius, (shell thickness)/(core radius), at the molecule−solvent interface. The form factor $P(q)$ of star-PS-6 in the high q region was dominated by density fluctuations on length scales smaller than the dimension of the star-PS-6 molecule. The scattering profile in the high q region most likely arose from the internal chain structures of the star-PS-6 arms. The motion of the star-PS-6 arms could be described as the self-avoiding random walk of an excluded volume chain, which consisted of "blobs",[39] where a "blob" is a spherical volume with radius ξ, where ξ is the correlation length of the density fluctuation. The blobs significantly influenced the scattering profile in the high q region. It should be noted that the $q^{-5/3}$ power law in the high q region of the scattering profile collected in cyclohexane was different from the power law (q^{-2}) of linear-PS in the Θ solvent. This difference was attributed to temperature effects and chain interactions.[15,40] Cyclohexane at 35 °C,

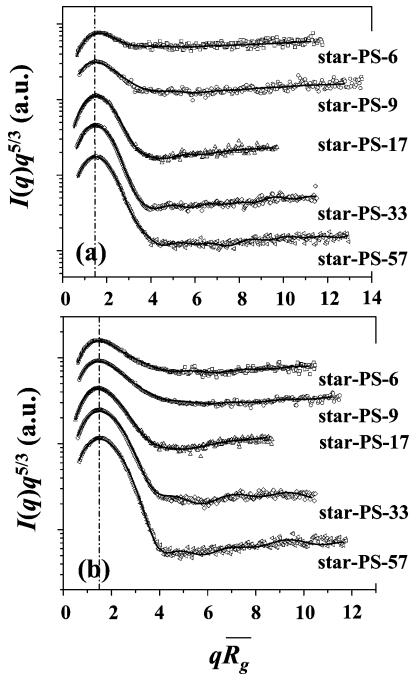

Figure 3. Modified Kratky representation of the SAXS profiles of the star-PS polymers, measured in (a) THF (good solvent) and (b) cyclohexane (Θ solvent).

which is a Θ solvent for linear-PS, yielded apparently somewhat different Θ solvent conditions for the star-PS-6 polymer.

The overall molecular shape of star-PS-6 was determined from a structural model analysis of the measured scattering profiles. A functional description of the form factor can be proposed for star molecules with high functionality:[23]

$$P(q) = P_{\text{star}}(q) + 4\pi\alpha \int_0^{\bar{\xi}} r^2 \gamma(r) \frac{\sin(qr)}{qr}\, dr \qquad (10)$$

where $\gamma(r)$ describes the density fluctuations on length scales smaller than the blob radius, and α is the amplitude of the blob scattering contribution. The first term in $P_{\text{star}}(q)$ is the form factor for the star molecule, and the second term $P_{\text{blob}}(q)$ is the Fourier transform of the density correlation function $\gamma(r)$. In eq 10, the correlation function of the density fluctuations is equal to zero for length scales larger than the correlation length $\bar{\xi}$ and, therefore, the integral is nonzero for $r \leq \bar{\xi}$. According to previous results[41] for $r \leq \bar{\xi}$, $\gamma(r)$ can be expressed by

$$\gamma(r) \propto r^{\mu-2} \qquad (11a)$$

$$\mu = \upsilon^{-1} - 1 \qquad (11b)$$

where υ is the Flory−Huggins parameter, which equals 3/5 for good solvents, 1/2 for Θ solvents, and 2/3 for stretched molecules. Therefore, the blob should contribute significantly to the scattering profile in the high q region (Figure 4a).

In eq 10, two structural models (fuzzy sphere and fuzzy ellipsoid) were tested to solve for the form factor $P_{\text{star}}(q)$ of the star-PS-6. Here, both models consist of two parts, a spherical (or ellipsoidal) core and a soft outer region. In the fuzzy sphere model, $P_{\text{star}}(q)$ can be replaced by

$$P_{\text{f}}^{\text{sph}}(q,R_{\text{f}},\sigma_{\text{f}}) = A_{\text{f}}^{\text{sph}}(q,R_{\text{f}},\sigma_{\text{f}})^2 \qquad (12a)$$

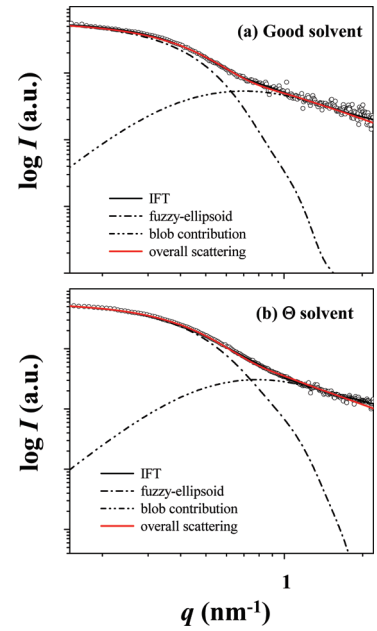

Figure 4. SAXS profiles of star-PS-6 in (a) good solvent (THF) and (b) Θ solvent (cyclohexane). The symbols indicate the measured data; the solid lines indicate the IFT fit. The measured scattering profiles could be fit well to a fuzzy ellipsoid model; in the high q region, the scattering profiles were significantly influenced by the blob morphology of the arms. The concentrations of the polymer solutions were 1.0 wt %.

$$A_{\text{f}}^{\text{sph}}(q,R_{\text{f}},\sigma_{\text{f}}) = A_{\text{sphere}}(q,R_{\text{f}}) \exp\left(-\frac{q^2\sigma_{\text{f}}^2}{4}\right) \qquad (12b)$$

where R_{f} is the radius of the spherical core, which is related to the radius of gyration by $R_{\text{s}} = (3/5)^{1/2}R_{\text{f}}$, $2\sigma_{\text{f}}$ is a measure of the width of the soft shell region (the soft shell thickness), and A_{sphere} is the scattering amplitude of the hard sphere with the same mass and core density. The fuzzy ellipsoid model contains an ellipsoidal core with main axes R_{m}, R_{m}, and εR_{m} (here, ε is the aspect ratio, the (short axis)/(long axis)), and the form factor of the core can be expressed by

$$P_{\text{core}}^{\text{ell}}(q,\varepsilon,R_m) = \int_0^{\pi/2} P_{\text{sphere}}(q,r) \sin\alpha\, d\alpha \qquad (13a)$$

$$r = R_{\text{m}}\sqrt{\sin^2\alpha + \varepsilon^2\cos^2\alpha} \qquad (13b)$$

where P_{sphere} is the form factor of the hard sphere.[42] Thus, the form factor $P_{\text{star}}(q)$ of the fuzzy ellipsoid must be replaced by

$$P_{\text{f}}^{\text{ell}}(q,\varepsilon,R_{\text{m}},\sigma_{\text{f}}) = A_{\text{f}}^{\text{ell}}(q,\varepsilon,R_{\text{m}},\sigma_{\text{f}})^2 \qquad (14a)$$

$$A_{\text{f}}^{\text{ell}}(q,\varepsilon,R_{\text{m}},\sigma_{\text{f}}) = A_{\text{core}}^{\text{ell}}(q,\varepsilon,R_{\text{m}}) \exp\left(-\frac{q^2\sigma_{\text{f}}^2}{4}\right) \qquad (14b)$$

where $A_{\text{core}}^{\text{ell}}$ is the scattering amplitude of the ellipsoidal core: $A_{\text{core}}^{\text{ell}}(q,\varepsilon,R_m)^2 = P_{\text{core}}^{\text{ell}}(q,\varepsilon R_m)$. Here the radius of gyration of the ellipsoidal core is given by $R_{\text{e}} = R_{\text{m}}[(2+\varepsilon^2)/5]^{1/2}$.

The experimental scattering profiles were modeled using the fuzzy sphere and fuzzy ellipsoid models described above. The scattering profiles measured in both solvents fit well to the fuzzy

TABLE 3: Molecular Shapes and Characteristics of the Star-PS Polymers

		THF				cyclohexane			
star-PS polymer	molecular shape[a]	R_f[b] (Å)	ε[c]	σ_f/R_f[d] (%)	D_{max}[e] (Å)	R_f[b] (Å)	ε[c]	σ_f/R_f[d] (%)	D_{max}[e] (Å)
star-PS-6	fuzzy-ellipsoid	38	0.20	36.8	140.0	36	0.11	41.7	130.0
star-PS-9	fuzzy-ellipsoid	45	0.21	35.6	167.4	37	0.18	43.2	148.5
star-PS-17	fuzzy-ellipsoid	30	0.53	50.0	118.8	27	0.44	51.9	103.5
star-PS-33	fuzzy-sphere	54	~1.0	31.0	112.8	48	~1.0	29.7	102.2
star-PS-57	fuzzy-sphere	58	~1.0	27.5	134.4	53	~1.0	25.0	118.8

[a] Molecular shape determined from the SAXS data analysis. [b] Radius of gyration of core. [c] Aspect ratio [=(short axis)/(long axis)]. [d] Fuzziness: here σ_f is the shell thickness in a fuzzy-ellipsoid or a fuzzy-sphere. [e] The maximum dimension of star-PS determined by the pair distance function analysis of measured scattering data.

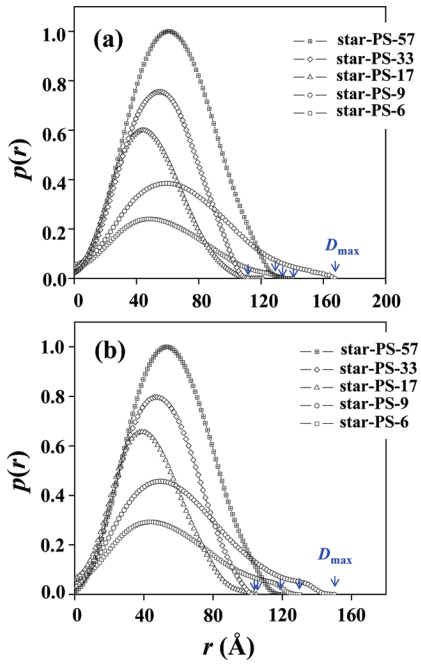

Figure 5. Pair distance distribution functions $p(r)$ of star-PS polymers under (a) good (THF) and (b) Θ (cyclohexane) solvents, determined from the measured X-ray scattering data using IFT analysis.

ellipsoid model, as shown in Figure 4a. The scattering profiles in the high q region were influenced by the contributions of the blobs. The model-independent IFT method fit well to the entire region of both scattering profiles (Figures 2 and 4a). These results suggested that the star-PS-6 polymer, under either solvent condition, was best described as an ellipsoidal core with a thick shell, and therefore, its overall shape was a fuzzy ellipsoid. The fuzziness was measured to be 36.8−41.7%, depending on the solvent. The structural parameters obtained are summarized in Table 3.

With the above structural information, the pair correlation function and radial density distribution were extracted from the scattering data to estimate additional structural details of the star-PS-6. The pair correlation function $p(r)$, which can be obtained from the scattering data by IFT analysis, is related to the radial electron density distribution function $\rho(r)$ by the following expression:[27–30]

$$p(r) = r^2 \int_{-\infty}^{\infty} \rho(r)\, \rho(x-r)\, \mathrm{d}x \qquad (15)$$

Figure 5 shows the $p(r)$ profiles determined from the experimental scattering data. As can be seen in the figure, the star-PS-6 polymer, in both solvents, revealed an asymmetric $p(r)$ profile. The maximum dimension (D_{max}) was estimated from the $p(r)$ profiles. The resulting parameters are listed in Table 3. The asymmetric $p(r)$ profile, as well as the relatively large D_{max} values for the star-PS-6 lent further support to the ellipsoidal structural model. The $\rho(r)$ profiles are shown in Figure 6. The $\rho(r)$ profiles suggest that star-PS-6 consists of a dense core and a less dense shell.

Taking into account the structural characteristics determined above, we propose that a fuzzy ellipsoidal model describes the three-dimensional (3D) molecular shape for the star-PS-6 polymer in both good and Θ solvents. Figure 7 shows the core and shell 3D fuzzy ellipsoidal structure.

The solution-based ellipsoidal structure for star-PS-6 was unexpected, because the star polymer has a $\bar{M}_w$ of 68 800 and contains 6 arms, each of which has a $\bar{M}_w$ of 11 460 per arm. PS is a flexible polymer, and even the shape of linear-PS can be described as a Gaussian sphere in solution. Therefore, star-PS-6 was expected to have a spherical shape. In our study, the ellipsoidal shape may be attributed to the molecular architecture and the limited number of arms. As can be seen in Figure 1, the 6 arms in the polymer are attached at 6 different positions rather than at a single point. The first two arms are connected near the center of the molecule; to the starting point of an arm are attached two more arms. A third set of two arms are connected to the second two arms' starting points. The extended anisotropic branches formed by the 6 arms yield a high aspect ratio and, therefore, an ellipsoidal molecular structure. The effect of the extended branched connections may be reduced by increasing the number of arms.

9-Armed Star-PS (Star-PS-9). The SAXS profiles of star-PS-9 in THF and in cyclohexane are shown in Figure 2. The scattering profiles in both solvents were similar to those of star-PS-6. However, the scattering profiles of star-PS-9 were shifted slightly toward the low q region, compared to those of star-PS-6, suggesting that the structure of star-PS-9 closely resembled that of the 6-arm PS, despite the increase in molecular size.

As can be seen in Figure 2, the star-PS-9 scattering profiles were fit well by the model-independent IFT method. The molecular sizes of star-PS-9 in each solvent were obtained from the Guinier fit and the IFT method. The fit parameters are listed in Table 2. Overall, the $\bar{R}_g$ values were larger than those of star-PS-6, indicating that the size of star-PS molecules increased with the number of arms. SAXS analysis indicated that star-PS-9 molecules were larger in the good solvent than in the Θ solvent, as expected. The R_g value determined by IFT was smaller than that estimated by the Guinier analysis, as was observed for star-PS-6. This discrepancy indicated that the star-PS-9 molecular shape contained anisotropic character. The g values agreed with the theoretical values in both good and Θ solvents, indicating that the star-PS-9 polymer revealed a starlike molecular behavior in both good and Θ solvents.

In the intermediate q region (Figure 2), the scattering profiles measured in both solvents were similar to the corresponding

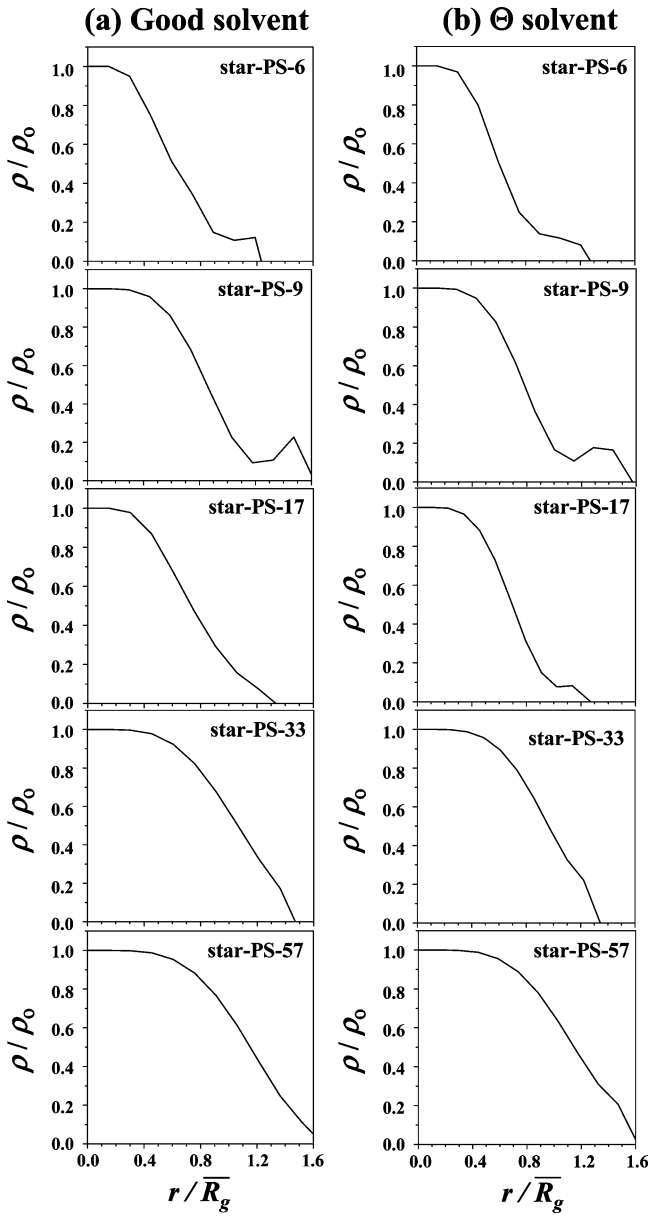

Figure 6. Density distribution functions $\rho(r)$ of star-PS polymers under (a) good (THF) and (b) Θ (cyclohexane) solvents, determined from the measured X-ray scattering data using IFT analysis. The y-axis of $\rho(r)$ was normalized to its maximum value; the x-axis was normalized to the $\bar{R}_g$ value determined from the Guinier analysis of the measured scattering data.

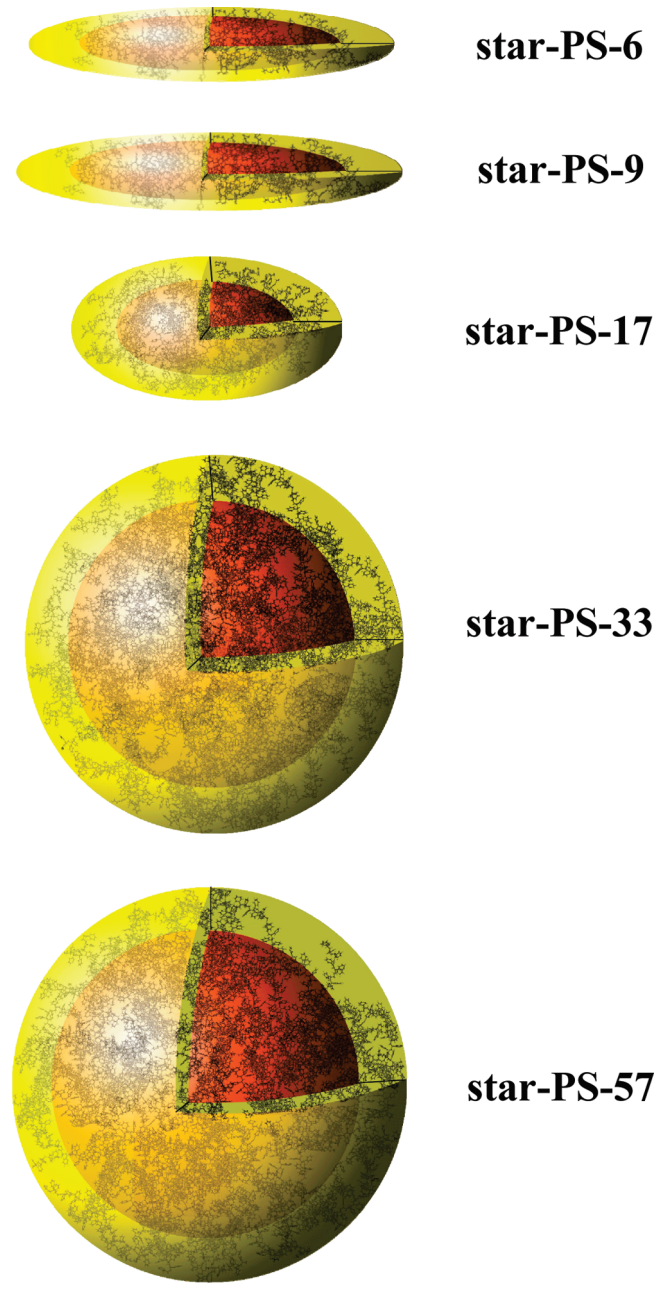

Figure 7. Three-dimensional molecular shapes of the star-PS polymers under good solvent (THF) conditions; the structural parameters were determined from analysis of the X-ray scattering data: star-PS-6, star-PS-9, star-PS-17, star-PS-33, and star-PS-57.

solvent scattering profiles of star-PS-6, suggesting that the molecular shapes were also similar. However, the overall molecular shape of star-PS-9 was different from that of star-PS-6 in that star-PS-9 molecules were more compact than star-PS-6 molecules. This difference is apparent in the plot of $I(q)q^{5/3}$ versus $q\bar{R}_g$, as shown in Figure 3. In the plot, star-PS-9 reveals a maximum more near $q\bar{R}_g = 1.49$, compared to star-PS-6, but not exactly at $q\bar{R}_g = 1.49$. Therefore, the molecular shape of star-PS-9 was not a homogeneous sphere.

In the high q region (Figure 2), the scattering profiles of star-PS-9 in both solvents followed a power law distribution consistent with a description of the intra-arm diffusion as a self-avoiding random walk with excluded volume effects. The scattering profile measured in cyclohexane followed a $q^{-5/3}$ power law distribution, indicating that temperature effects and chain interactions influenced the solution behavior.

The above results suggested that the star-PS-9 polymer could also be described by a fuzzy ellipsoid model in both the good and the Θ solvent. The star-PS-9 fuzzy ellipsoid was larger than that of the star-PS-6: its fuzziness was lower, and the core was larger than in the star-PS-6. The star-PS-9 polymer revealed a theoretically starlike molecular behavior in both good and the Θ solvents, as observed for star-PS-6. The structural parameters are listed in Table 3.

The pair correlation function and radial density distribution were calculated from the star-PS-9 scattering data to extract a more detailed description of the overall molecular shape. Figure 5 shows the $p(r)$ profiles for star-PS-9. The $p(r)$ profiles are asymmetric, showing a large D_{max} value. The fit parameters are listed in Table 3. The asymmetric $p(r)$ profiles, as well as the large D_{max} values support a highly ellipsoidal model as a

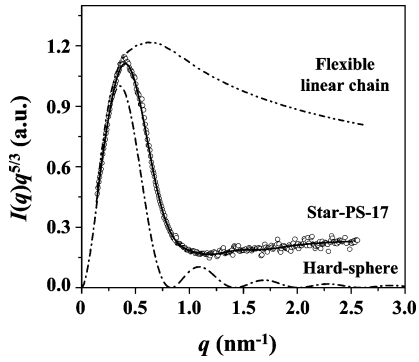

Figure 8. Modified Kratky representation of the scattering profile of star-PS-17 under good solvent (THF) conditions, compared to the theoretically predicted plots for the flexible linear chain and the hard sphere models. The solid line was obtained by fitting the scattering data using the IFT method.

reasonable description for star-PS-9. The $\rho(r)$ profiles indicate the presence of a dense core and a less dense shell (Figure 6).

The structural characteristics collectively support a 3D fuzzy ellipsoidal structure for the 9-armed star-PS-9 polymer in both good and Θ solvents (Figure 7). The 9 arms of the star-PS-9 polymer were unable to compensate for the radial effects of the extended branched connections, and an ellipsoidal shape resulted.

17-Armed PS (Star-PS-17). The scattering profiles of star-PS-17 were measured in both good and Θ solvents, as shown in Figure 2. The scattering profiles are quite different from those of the star-PS-6 and star-PS-9 polymers, indicating that the star-PS-17 polymer assumed a different molecular shape.

With 17 arms, one would expect that the solution structure of star-PS-17 would be larger in size than those of star-PS-6 and star-PS-9. However, the star-PS-17 polymer was characterized by a smaller $\bar{R}_g$ than either star-PS-6 or star-PS-9 (Table 2), because the star-PS-17 arms were lower in molecular weight (Table 2) than the arms of star-PS-6 and star-PS-9. The g values of star-PS-17 (Table 2) suggested a theoretically starlike molecular solution behavior in the good and the Θ solvents, similar to star-PS-6 and star-PS-9.

In the intermediate q region, the scattering profiles closely followed a q^{-4} power law rather than a $q^{-5/3}$ power law (Figure 2). A plot of $I(q)q^{5/3}$ versus $q\bar{R}_g$ (Figure 3) presented a maximum very near $q\bar{R}_g = 1.49$, compared to star-PS-6 and star-PS-9, but not exactly at $q\bar{R}_g = 1.49$. These results collectively indicated that the star-PS-17 polymer assumed an ellipsoidal shape with an angular eccentricity (aspect ratio) approaching that of a sphere.

The scattering profile of star-PS-17, measured in good solvent, was analyzed as follows: the intensity was multiplied by $q^{5/3}$, and the product was plotted against q and then compared with the same function calculated for the linear-PS (i.e., a Gaussian sphere) and a hard sphere model in which the $\bar{R}_g$ was set equal to that of the star-PS-17 polymer. Figure 8 shows that the flexible linear-PS polymer chain followed a q^{-2} power law behavior in the high q region, attributed to the Gaussian condition, whereas the hard sphere followed a q^{-4} power law, attributed to the presence of a sharp particle−solvent interface. The scattering profile of the star-PS-17 in the high q region followed a $q^{-5/3}$ power law, suggesting that the intra-arm diffusion in the star-PS-17 polymer chain could be modeled as a self-avoiding random walk in which the blob contribution was significant. Overall, the scattering profile of the star-PS-17 polymer more closely resembled that of a hard sphere than that

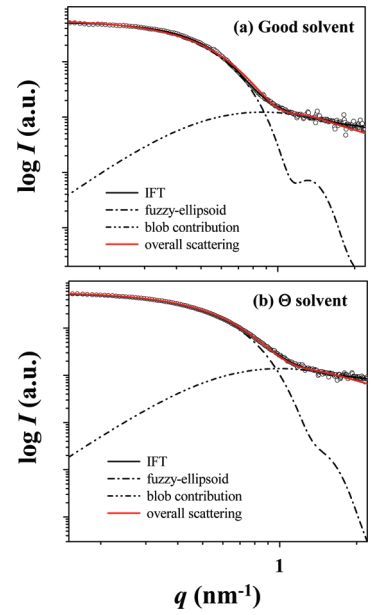

Figure 9. SAXS profiles of star-PS-17 in (a) good solvent (THF) and (b) Θ solvent (cyclohexane). The symbols indicate the measured data; the solid line was obtained by fitting the data using the IFT method. The measured scattering profiles also fit well to a fuzzy ellipsoid model; in the high q region, the scattering profiles were significantly influenced by the blob morphology of the arms. The concentrations of the polymer solutions were 1.0 wt %.

of the linear-PS. Similar results were obtained from star-PS-17 in the Θ solvent (data not shown).

The scattering profiles of star-PS-17 were fit to several structural models, including the hard sphere, the fuzzy sphere, and the fuzzy ellipsoid. The scattering profiles measured in both solvents fit well to a fuzzy ellipsoid model (Figure 9). Figure 9 shows that the contribution of the blobs was significant in the high q region of the scattering profiles. The model-independent IFT method fit all regions of the scattering profiles well. These results suggest that the star-PS-17 polymer, in both solvents, had a fuzzy ellipsoidal shape that was very nearly a fuzzy sphere. The obtained structural parameters are summarized in Table 3.

Figures 5 and 6 show the $p(r)$ and $\rho(r)$ profiles of star-PS-17 in both good and Θ solvents. The $p(r)$ profiles were more symmetric than those of star-PS-6 and star-PS-9. The D_{max} values were much smaller than those of star-PS-6 and star-PS-9. The $\rho(r)$ profiles also clearly indicated that the star-PS-17 polymer structure consisted of a dense core and a less dense shell.

The structural characteristics suggest a 3D fuzzy ellipsoidal structural model for the star-PS-17 polymer in both good and Θ solvents (Figure 7). The star-PS-17 polymer revealed a fuzzy ellipsoidal shape, indicating that the effects of the extended branched attachments were significant even in the presence of the space filling effects of the 17 arms. However, the ellipsoidal shape of star-PS-17 was somewhat different from the shapes of star-PS-6 and star-PS-9. In particular, the aspect ratio ε of the fuzzy ellipsoid was much larger than those of the star-PS-6 and star-PS-9 (Table 3). The fuzziness of the star-PS-17 polymer was also much larger than the fuzziness of star-PS-6 and star-PS-9 (Table 3).

33-Armed PS (Star-PS-33). Figure 2 shows that the scattering profiles of star-PS-33, measured in the good and Θ solvents, were similar in shape (with a few significant differences) to those of star-PS-17 but were quite different from those of star-PS-6 and star-PS-9. The scattering analysis results are summarized in Table 2.

The $\bar{R}_g$ values of star-PS-33, in both solvents, were larger than those of star-PS-17, but smaller than those of star-PS-6 and star-PS-9. These observations can be explained as follows. The arms of star-PS-33 and star-PS-17 were nearly identical in terms of the number of segments and, therefore, were shorter than the arms of star-PS-6 and star-PS-9. The star-PS-33 molecule had a more limited ability to expand in solution due to its dense inner structure than star-PS-17.

In both solvents, the g values for star-PS-33 agreed well with the theoretical values. The scattering profiles of the polymer, in both solvents, followed a q^{-4} power law in the intermediate q region. A plot of $I(q)q^{5/3}$ versus $q\bar{R}_g$ revealed a maximum very close to $q\bar{R}_g = 1.49$ (Figure 3). These results collectively indicated that the molecular shape of star-PS-33 could be described as a hard sphere with starlike molecular behavior. However, the contribution of the blobs was clearly discernible in the high q region of the scattering profiles, indicating that the star-PS-33 molecule presented fuzzy characteristics as well.

The scattering profiles of star-PS-33 were fit to several structural models, with the best fit provided by the fuzzy sphere rather than the fuzzy ellipsoid. The model-independent IFT method yielded a good fit to the full scattering profiles. The star-PS-33 polymer, in both solvents, could be described by a fuzzy sphere model consisting of a core and shell parts. The shell region was smaller than that of the star-PS-17 polymer (i.e., the fuzziness of star-PS-33 was 29.7−31.0%) depending on the solvent. The structural parameters are summarized in Table 3.

The $p(r)$ and $\rho(r)$ profiles of star-PS-33, which were determined by IFT analysis, are shown in Figures 5 and 6, respectively. The $p(r)$ profiles were symmetric, with a bell shape (Figure 5). The D_{max} values were much smaller than those of star-PS-6, star-PS-9, and star-PS-17. The $\rho(r)$ profiles also showed that the star-PS-33 polymer consisted of a dense core and a less dense shell.

The structural characteristics collectively suggest that a 3D fuzzy spherical structure described the star-PS-33 polymer in both good and Θ solvents (Figure 7). The star-PS-33 polymer was best modeled as a fuzzy sphere rather than a fuzzy ellipsoid, indicating that the effect of the extended branched connections of the chemical architecture were completely compensated by the space filling effects of the 33 arms.

57-Armed PS (Star-PS-57). The star-PS-57 polymer, in both good and Θ solvents, showed scattering profiles similar, in shape, to those of star-PS-17 and star-PS-33 (Figure 2). However, some features of the scattering profiles differed from those of star-PS-17 and star-PS-33. The scattering analysis results are summarized in Table 2.

The $\bar{R}_g$ values for star-PS-57 in both solvents were larger than those of star-PS-17 and star-PS-33. The arms in star-PS-57 were nearly identical to the arms in star-PS-17 and star-PS-33, in terms of the number of segments (Table 2). A comparison of the molecular dimensions of star-PS-17, star-PS-33, and star-PS-57 polymers, shows a steady increase with the increasing number of arms. In both solvents, the g values agreed well with the theoretical values. The scattering profiles in both solvents closely followed a q^{-4} power law in the intermediate q region. A plot of $I(q)q^{5/3}$ versus $q\bar{R}_g$ revealed a maximum very near $q\bar{R}_g = 1.49$ and, moreover, first-, second-, and third-order minima at $q\bar{R}_g = 3.65$, 6.08, and 8.52 (Figure 3), which are characteristic of a hard sphere: $q\bar{R}_g = (3/5)^{1/2}(2n + 1)\pi/2$, where n is the order number of the minima. These results collectively indicate that the molecular shape of star-PS-57 can be described as a hard sphere with starlike molecular behavior. However, the contributions of the blobs were discernible in the high q region of the scattering profiles, suggesting that the star-PS-57 molecule in both solvents presented fuzzy characteristics as well.

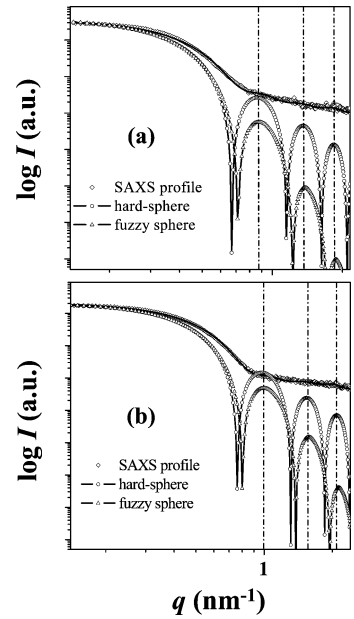

Figure 10. SAXS profiles of star-PS-57 in (a) good solvent (THF) and (b) Θ solvent (cyclohexane): the diamond symbols indicate the measured data; the solid line was obtained by fitting the data using the IFT method; the circles indicate the scattering profile calculated using the fuzzy sphere model; the triangles indicate the scattering profile calculated using the hard sphere model. The structural parameters were determined from analysis of the X-ray scattering data. The concentrations of the polymer solutions were 1.0 wt %.

The scattering profiles of star-PS-57 measured in both solvents were fit to various structural models, including the hard sphere, the fuzzy sphere, and the fuzzy ellipsoid. The fuzzy sphere yielded a better fit to the scattering data than did the fuzzy ellipsoid (Figure 10). The model-independent IFT method yielded a good fit to the full scattering profiles. These results indicate that the star-PS-57 polymer in both solvents can be described as a fuzzy sphere consisting of core and shell parts. However, the shell thickness of the star-PS-57 polymer was smaller than the shells of star-PS-17 and star-PS-33 polymers. The structural parameters are summarized in Table 3.

Figures 5 and 6 show the $p(r)$ and $\rho(r)$ profiles of star-PS-57, respectively. The $p(r)$ profiles are symmetric, with a bell shape (Figure 5). The D_{max} values are much smaller than those of star-PS-6 and star-PS-9, but larger than those of star-PS-17 and star-PS-33. The $\rho(r)$ profiles also suggest that the star-PS-57 polymer consists of a dense core and a less dense shell.

The structural characteristics collectively suggest that a 3D fuzzy sphere structural model best describes the shape of star-PS-33 polymers in good and Θ solvents (Figure 7). The star-PS-57 polymer assumed a fuzzy sphere rather than a fuzzy ellipsoid shape. The star-PS-57 was characterized by the lowest fuzziness (25.0−27.5%), indicating that the effect of the extended branched connections that result from the chemical architecture were completely compensated by the space filling effect of the 57 arms.

Conclusions

We investigated the structure and shapes of well-defined star-PS polymers with 6, 9, 17, 33, and 57 arms in good and Θ

solvents using SAXS with a synchrotron radiation source. The SAXS data revealed details of the molecular sizes and shapes of the star-PS polymer series, including blob contributions, the radius of gyration, the pair distributions, radial electron density distributions, and the Zimm−Stockmayer and Roovers *g*-factors.

The molecular size and shape of the star-PS polymers varied with the number of arms. The radii of gyration of star-PS polymers ranged from 30.2 to 49.5 Å, depending on the number of arms, the solvent, and the molecular weights. The shapes of the star-PS polymers containing 6, 9, or 17 arms could be described as fuzzy ellipsoids, consisting of a core and a shell. The aspect ratio decreased with the increasing number of arms. The fuzziness ranged from 35.6 to 51.9%, depending on the number of arms and the solvent. The ellipsoidal molecular shapes were favored at lower arm numbers by the extended anisotropic architecture of the connection part of arms. The effect of the extended anisotropic branches decreased as the number of arms increased, because the space-filling effects of the arms became more significant. In contrast, the star-PS polymers with 33 or 57 arms could be described as fuzzy spheres. The fuzziness ranged from 25.0 to 31.0%, depending on the number of arms and the solvent. The spherical shapes indicated that with sufficient (>33) arms, the effects of the extended anisotropically branched connections in the molecular architecture were compensated by the space filling effects of the large number of arms.

The arms in the star-PS polymer were found to be more extended than the arms in the linear-PS polymer. The degree of chain extension in the arms increased with increasing the number of arms.

Acknowledgment. This study was supported by the National Research Foundation of Korea (Korea-Japan Cooperation Project No. 4000186001, National Research Lab Program, the Center for Electro-Photo Behaviors in Advanced Molecular Systems), and the Ministry of Education, Science & Technology (MEST) (BK21 Program and World Class University Program). A.H. gratefully acknowledges the financial support for this work from a Grant-in-Aid for Scientific Research (No. (B) 21350060) from the Ministry of Education, Science, Sports, and Culture of Japan. T.H. is thankful for support from the Japan Society for the Promotion of Science Research Fellowships for Young Scientists. The SAXS measurements at Pohang Accelerator Laboratory were supported by the MEST, POSCO, and POSTECH Foundation.

References and Notes

(1) (a) Jansen, J. F. G. A.; Peerlings, H. W. I.; de Brabander-Van den Berg, E. M. M.; Meijer, E. W. *Angew. Chem.* **1995**, *34*, 1206. (b) Tabakovic, I.; Miller, L. L.; Duan, R. G.; Tully, D. C.; Tomalia, D. A. *Chem. Mater.* **1997**, *9*, 736. (c) Groll, J.; Amirgoulova, E. V.; Ameringer, T.; Heyes, C. D.; Rocker, C.; Nienhaus, G. U.; Moller, M. *J. Am. Chem. Soc.* **2004**, *126*, 4234.

(2) Jiang, D.-L.; Aida, T. *Nature* **1997**, *388*, 454.

(3) (a) Hirao, A.; Hayashi, M.; Loykulnant, S.; Sugiyama, K.; Ryu, S.-W.; Haraguchi, N.; Matsuo, A.; Higashihara, T. *Prog. Polym. Sci.* **2005**, *30*, 111. (b) Hirao, A.; Sugiyama, K.; Yokoyama, H. *Prog. Polym. Sci.* **2007**, *32*, 1393.

(4) (a) Shin, Y. C.; Choi, K.-Y.; Jin, M. Y.; Hong, S.-K.; Cho, D.; Chang, T.; Ree, M. *Korea Polym. J.* **2001**, *9*, 100. (b) Kim, J.-S.; Kim, H.-C.; Lee, B.; Ree, M. *Polymer* **2005**, *46*, 7394.

(5) (a) Lee, B.; Park, Y.-H.; Hwang, Y.-T.; Oh, W.; Yoon, J.; Ree, M. *Nat. Mater.* **2005**, *4*, 147. (b) Lee, B.; Oh, W.; Hwang, Y.; Park, Y.-H.; Yoon, J.; Jin, K. S.; Heo, K.; Kim, J.; Kim, K.-W.; Ree, M. *Adv. Mater.* **2005**, *17*, 696. (c) Lee, B.; Yoon, J.; Oh, W.; Hwang, Y.; Heo, K.; Jin, K. S.; Kim, J.; Kim, K.-W.; Ree, M. *Macromolecules* **2005**, *38*, 3395. (d) Lee, B.; Oh, W.; Yoon, J.; Hwang, Y.; Kim, J.; Landes, B. G.; Quintana, J. P.; Ree, M. *Macromolecules* **2005**, *38*, 8991. (e) Ree, M.; Yoon, J.; Heo, K. *J. Mater. Chem.* **2006**, *16*, 685. (f) Heo, K.; Jin, K. S.; Yoon, J.; Jin, S.; Oh, W.; Ree, M. *J. Phys. Chem. B* **2006**, *110*, 15887. (g) Yoon, J.; Heo, K.; Oh, W.; Jin, K. S.; Jin, S.; Kim, J.; Kim, K.-W.; Chang, T.; Ree, M. *Nanotechnology* **2006**, *17*, 3490. (h) Oh, W.; Park, Y. D.; Hwang, Y.; Ree, M. *Bull. Korean Chem. Soc.* **2007**, *28*, 2481.

(6) Bauer, B. J.; Fetters, L. J. *Rubber Chem. Technol.* **1978**, *51*, 406.

(7) (a) Fetters, L. J.; Tomas, E. L. In *Material Science and Technology*: VCH Verlangesellschaft: Weinheim, Germany, 1993; Vol. 12, p 1. (b) Grest, G. S.; Fetters, L. J.; Huang, J. S. *Adv. Chem. Phys.* **1996**, 67 XCIV.

(8) (a) Roovers. J. In *Encyclopedia of Polymer Science and Engineering*, 2nd ed.; Kroschwitz, J. I., ed.; Wiley-Interscience: New York, 1985; Vol. 2, p 478. (b) Rempp, P.; Herz, J. E. In *Encyclopedia of Polymer Science and Engineering*, 2nd ed.; Kroschwitz, J. I., ed.; Wiley-Interscience: New York, 1989; Supplemental Volume, p 493.

(9) Lutz, P. J.; Rein, D. In *Star and Hyperbranched Polymers*: Mishra, M. K., Kobayashi, S., Eds.; Marcel Dekker, Inc.: New York, Basel, 1999; p 27.

(10) (a) Pitsikalis, M.; Pispas, S.; Mays, J. W.; Hadjichristidis, N. *Adv. Polym. Sci.* **1998**, *135*, 1. (b) Hadjichristidis, N.; Pitsikalis, M.; Pispas, S.; Iatou, H. *Chem. Rev.* **2001**, *101*, 3747.

(11) Roovers, J.; Zhou, L. L.; Toporowski, P. M.; van der Zwan, M.; Iatrou, H.; Hadjichristidis, N. *Macromolecules* **1993**, *26*, 4324.

(12) Willner, L.; Jucknischke, O.; Richter, D.; Roovers, J.; Zhou, L.-L.; Toporowski, P. M.; Fetters, L. J.; Huang, J. S.; Lin, M. Y.; Hadjichristidis, N. *Macromolecules* **1994**, *27*, 3821.

(13) (a) Hadjichristidis, N.; Roovers, J. E. L. *J. Polym. Sci., Polym. Phys. Ed.* **1974**, *12*, 2521. (b) Roovers, J.; Hadjichristidis, N.; Fetters, L. J. *Macromolecules* **1983**, *16*, 214.

(14) Roovers, J.; Toporowski, P.; Martin, J. *Macromolecules* **1989**, *22*, 1897.

(15) Khasat, N.; Pennisi, R.; Hadjichristidis, N.; Fetters, L. *Macromolecules* **1988**, *21*, 1100.

(16) Bauer, B. J.; Fetters, L. J.; Graessley, W. W.; Hadjichristidis, N.; Quack, G. F. *Macromolecules* **1989**, *22*, 2337.

(17) Freire, J. J.; Pla, J.; Rey, A.; Prats, R. *Macromolecules* **1986**, *19*, 452.

(18) Douglas, J. F.; Roovers, J.; Freed, K. F. *Macromolecules* **1990**, *23*, 4168.

(19) Jin, S.; Higashihara, T.; Watanabe, T.; Jin, K. S.; Yoon, J.; Heo, K.; Kim, J.; Kim, K.-W.; Hirao, A.; Ree, M. *Macromol. Res.* **2008**, *16*, 686.

(20) Huber, K.; Burchard, W.; Fetters, L. J. *Macromolecules* **1984**, *17*, 541.

(21) Huber, K.; Bantle, S.; Burchard, W.; Fetters, L. J. *Macromolecules* **1986**, *19*, 1404.

(22) (a) Richter, D.; Farago, B.; Huang, J. S.; Fetters, L. J.; Ewen, B. *Macromolecules* **1989**, *22*, 468. (b) Richter, D.; Farago, B.; Fetters, L. J.; Huang, J. S.; Ewen, B. *Macromolecules* **1990**, *23*, 1845.

(23) Dozier, W. D.; Huang, J. S.; Fetters, L. J. *Macromolecules* **1991**, *24*, 2810.

(24) Pearson, D. S.; Helfand, E. *Macromolecules* **1984**, *17*, 888.

(25) Roovers, J. *Polymer* **1985**, *26*, 1091.

(26) Batoulis, J.; Kremer, K. *Macromolecules* **1989**, *22*, 4277.

(27) (a) In *Small Angle Scattering X-Ray*; Guinier, A., Fournet, G., Eds.; Wiley: New York, 1955. (b) Roe, R.-J. *Methods of X-Ray and Neutron Scattering in Polymer Science*; Oxford, University Press: New York, 2000.

(28) (a) In*Small Angle Scattering X-Ray*; Glatter, O., Kratky, O., Eds.; Academic Press: New York, 1982. (b) Glatter, O. *Acta Phys. Austriaca* **1977**, *47*, 83. (b) Glatter, O. *J. Appl. Crystallogr.* **1977**, *10*, 415. (c) Glatter, O. *J. Appl. Crystallogr.* **1980**, *13*, 577.

(29) (a) Jang, D. S.; Lee, H. J.; Lee, B.; Hong, B. H.; Cha, H. J.; Yoon, J.; Lim, K.; Yoon, Y. J.; Kim, J.; Ree, M.; Lee, H. C.; Choi, K. Y. *FEBS Lett.* **2006**, *280*, 4166. (b) Choi, J. M.; Kang, S. Y.; Bae, W. J.; Jin, K. S.; Ree, M.; Cho, Y. *J. Biol. Chem.* **2007**, *282*, 9941. (c) Kim, D. Y.; Jin, K. S.; Kwon, E.; Ree, M.; Kim, K. K. *Proc. Natl. Acad. Sci. U.S.A.* **2007**, *104*, 8779. (d) Lee, J. H.; Kang, G. B.; Lim, H.-H.; Jin, K. S.; Kim, S.-H.; Ree, M.; Park, C.-S.; Kim, S.-J.; Eom, S. H. *J. Mol. Biol.* **2008**, *376*, 308.

(30) (a) Jin, K. S.; Kim, D. Y.; Rho, Y.; Le, V. B.; Kwon, E.; Kim, K. K.; Ree, M. *J. Synchrotron Rad.* **2008**, *15*, 219. (b) Jin, K. S.; Rho, Y.; Kim, J.; Kim, H.; Kim, I. J.; Ree, M. *J. Phys. Chem. B* **2008**, *112*, 15821. (c) Jin, K. S.; Park, J. K.; Yoon, J.; Rho, Y.; Kim, J.-H.; Kim, E. E.; Ree, M. *J. Phys. Chem. B* **2008**, *112*, 9603. (d) Shin, S. R.; Jin, K. S.; Lee, C. K.; Kim, S. I.; Spinks, G. M.; So, I.; Jeon, J.-H.; Kang, T. M.; Mun, J. Y.; Han, S.-S.; Ree, M.; Kim, S. J. *Adv. Mater.* **2009**, *21*, 1907. (e) Jin, K. S.; Shin, S. R.; Ahn, B.; Heo, K.; Kim, S. J.; Ree, M. *J. Phys. Chem. B* **2009**, *113*, 1852.

(31) (a) Hirao, A.; Haraguchi, N. *Macromolecules* **2002**, *35*, 7238. (b) Hirao, A.; Tokuda, Y. *Macromolecules* **2003**, *36*, 6081. (c) Hirao, A.; Watanabe, T.; Ishizu, K.; Ree, M.; Jin, S.; Jin, K. S.; Deffieux, A.; Schappacher, M.; Carlotti, S. *Macromolecules* **2009**, *42*, 682.

(32) (a) Shin, T. J.; Lee, B.; Youn, H. S.; Lee, K.-B.; Ree, M. *Langmuir* **2001**, *17*, 7842. (b) Lee, B.; Shin, T. J.; Lee, S. W.; Lee, J. W.; Ree, M. *Macromol. Symp.* **2002**, *190*, 173. (c) Bolze, J.; Kim, J.; Huang, J.-Y.; Rah, S.; Youn, H.; Lee, B.; Shin, T.; Ree, M. *Macromol. Res.* **2002**, *10*, 2. (d) Lee, B.; Shin, T. J.; Lee, S. W.; Yoon, J.; Kim, J.; Youn, H. S.; Lee, K.-B.;

Ree, M. *Polymer* **2003**, *44*, 2509. (e) Lee, B.; Shin, T. J.; Lee, S. W.; Yoon, J.; Kim, J.; Ree, M. *Macromolecules* **2004**, *37*, 4174. (f) Ree, M.; Ko, I. S. *Phys. High Tech.* **2005**, *14*, 2.

(33) (a) Shin, T. J.; Ree, M. *J. Phys. Chem. B* **2007**, *111*, 13894. (b) Heo, K.; Yoon, J.; Jin, K. S.; Jin, S.; Sato, H.; Ozaki, Y.; Satkowski, M. M.; Noda, I.; Ree, M. *J. Phys. Chem. B* **2008**, *112*, 4571. (c) Yoon, J.; Kim, K.-W.; Kim, J.; Heo, J.; Jin, K. S.; Jin, S.; Shin, T. J.; Lee, B.; Rho, B.; Ahn, B.; Ree, M. *Macromol. Res.* **2008**, *16*, 575. (d) Ree, M.; Nam, S. H.; Yoon, M.; Kim, B.; Kim, K.-R.; Kang, T.-H.; Kim, J.-Y.; Kim, K.-J.; Shin, T. J.; Lee, H.-S.; Park, S.-J.; Kim, N.; Lee, K.-B.; Ko, I.-S.; Namkung, W. *Synchrotron Radiation News* **2009**, *22*, 4.

(34) (a) Yamakawa, H. In *Modern Theory of Polymer Solutions*; Harper & Row: New York, 1971. (b) Konishi, T.; Yoshizaki, T.; Saito, T.; Einaga, Y.; Yamakawa, H. *Macromolecules* **1990**, *23*, 290. (c) Alessandrini, J. L.; Carignano, M. A. *Macromolecules* **1992**, *25*, 1157. (d) Abe, F.; Einaga, Y.; Yoshizaki, T.; Yamakawa, H. *Macromolecules* **1993**, *26*, 1884. (e) Xie, Y.; Ludwig, K. F.; Bansil, R.; Gallagher, P. D.; Cao, X.; Morales, G. *Physica A* **1996**, *26*, 94.

(35) Zimm, B. H.; Stockmayer, W. H. *J. Chem. Phys.* **1949**, *17*, 1301.

(36) Zimm, B. H.; Kilb, R. W. *J. Polym. Sci.* **1959**, *37*, 19.

(37) Stockmayer, W. H.; Fixman, M. *Anal. N. Y. Acad. Sci.* **1953**, *57*, 334.

(38) Roovers, J. In *Star and Hyperbranched Polymers*; Mishra, M. K. Kobayashi, S., Eds.; Marcel Dekker: New York, 1999; p 285.

(39) Rathgeber, S.; Monkenbusch, M.; Kreitschmann, M.; Urban, V.; Brulet, A. *J. Chem. Phys.* **2002**, *117*, 4047.

(40) Roovers, J.; Bywater, S. *Macromolecules* **1974**, *7*, 443.

(41) Kotlarchyk, M.; Chen, S. H. *J. Chem. Phys.* **1983**, *79*, 2461.

(42) Pedersen, J. *Adv. Colloid Interface Sci.* **1997**, *70*, 171.

JP911928B